THE JOURNAL OF PHYSICAL CHEMISTRY LETTERS
A JOURNAL OF THE AMERICAN CHEMICAL SOCIETY

pubs.acs.org/JPCL

Letter

Extreme Ultraviolet Wave Packet Interferometry of the Autoionizing HeNe Dimer

Daniel Uhl, Andreas Wituschek, Rupert Michiels, Florian Trinter, Till Jahnke, Enrico Allaria, Carlo Callegari, Miltcho Danailov, Michele Di Fraia, Oksana Plekan, Ulrich Bangert, Katrin Dulitz, Friedemann Landmesser, Moritz Michelbach, Alberto Simoncig, Michele Manfredda, Simone Spampinati, Giuseppe Penco, Richard James Squibb, Raimund Feifel, Tim Laarmann, Marcel Mudrich, Kevin C. Prince, Giulio Cerullo, Luca Giannessi, Frank Stienkemeier, and Lukas Bruder*

Cite This: *J. Phys. Chem. Lett.* 2022, 13, 8470–8476

Read Online

ACCESS | Metrics & More | Article Recommendations | Supporting Information

ABSTRACT: Femtosecond extreme ultraviolet wave packet interferometry (XUV-WPI) was applied to study resonant interatomic Coulombic decay (ICD) in the HeNe dimer. The high demands on phase stability and sensitivity for vibronic XUV-WPI of molecular-beam targets are met using an XUV phase-cycling scheme. The detected quantum interferences exhibit vibronic dephasing and rephasing signatures along with an ultrafast decoherence assigned to the ICD process. A Fourier analysis reveals the molecular absorption spectrum with high resolution. The demonstrated experiment shows a promising route for the real-time analysis of ultrafast ICD processes with both high temporal and high spectral resolution.

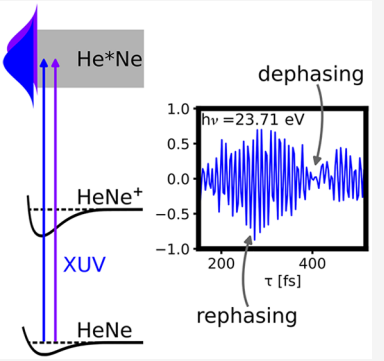

In wave packet interferometry (WPI), the interference between two optically prepared wavepackets is controlled and mapped using a sequence of ultrashort phase-locked laser pulses.[1] WPI is a key concept in coherent control,[2] high-resolution metrology,[3] and ultrafast multidimensional spectroscopy.[4,5] However, corresponding interferometric concepts are very scarce in the extreme ultraviolet (XUV) and X-ray spectral domains, despite many promising theory proposals for such experiments.[6] The major technical obstacles are (i) the demand for extreme phase stability to perform XUV/X-ray WPI and (ii) the lack of selective/background-free probes to recover the weak nonlinear signals of interest. These ingredients were demonstrated in separate experiments: on the one hand, in XUV and soft X-ray interferometry,[7−15] and on the other hand, in background-free near-infrared (NIR)-XUV/X-ray four-wave-mixing schemes.[16−19] Only recently, the combination of both ingredients was achieved in a single experiment by introducing a phase-cycling concept for XUV pulses.[10,11] A recent stability improvement of this scheme even shows promise for extensions to interferometric X-ray experiments.[20] These achievements lay the basis for the flexible implementation of various nonlinear spectroscopy concepts in the short-wavelength domain.

The few all-XUV interferometry experiments reported so far were restricted to the detection of electronic coherences in isolated atoms.[7,10,12,14] In contrast, molecular systems are much more complex, in particular when high-lying states in the XUV absorption region are studied, featuring typically a high density of electronic, vibrational, and rotational neutral and intermixing cationic states. In these systems, all-XUV interferometry could so far only access the beat spectra between different excited states[21,22] which provide only relative spectral information and thus can lead to ambiguities in the spectral assignments. The same issue applies to XUV-NIR interferometry, which is more frequently performed[23] due to the lower demands on phase stability and the circumvention of XUV beamline interferometers. In a recent demonstration, XUV-IR Raman interferometry was combined with photoelectron spectroscopy (PES) which lifted the degeneracy in the beat spectra with high resolution.[24] A related coherent multidimensional PES scheme has been demonstrated in the visible spectral domain.[25] Yet, so far these schemes were only demonstrated for atomic targets. They will be much more

Received: May 27, 2022
Accepted: August 4, 2022
Published: September 2, 2022

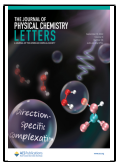

https://doi.org/10.1021/acs.jpclett.2c01619
J. Phys. Chem. Lett. 2022, 13, 8470−8476

difficult to implement for more advanced systems, e.g., molecules, where the large number of cationic states usually causes a congestion of the photoelectron spectra. In contrast, all-XUV interferometry with sufficient phase stability and sensitivity to directly track the beatings between the system's excited and the initial ground states solves these issues. Here, absolute frequency information correlated to the ground state is gained without the need of advanced electron detectors or knowledge of the system's cationic sates. In this letter, we demonstrate the latter approach and track the complex response of vibronic WPs in autoionizing states of a molecule using all-XUV interferometry.

Autoionization has been extensively studied in isolated atoms and is caused by the configuration interaction between the electrons of the atom leading to the famous Fano resonance lineshapes.[26] In weakly bound matter, such as, e.g., van der Waals clusters, interatomic Coulombic decay (ICD) offers an additional decay mechanism mediated by interparticle dipolar interactions,[27] which has been extensively studied in recent years.[28] Resonant ICD may occur if the resonantly excited bound state of one atom is energetically embedded in the ionization continuum of another atom in the system. This process has been studied in the HeNe heterodimer using frequency-domain spectroscopy.[29] Here, we apply XUV-WPI to track the ultrafast decoherence of electronic WPs caused by the resonant ICD process. In contrast to frequency-domain spectroscopy, this approach opens up the possibility to study ICD and related ultrafast conversion processes in real time with high spectral and temporal resolution.

Figure 1 shows schematically the probed ICD process in the HeNe dimer. The two rare-gas atoms form a weakly bound van

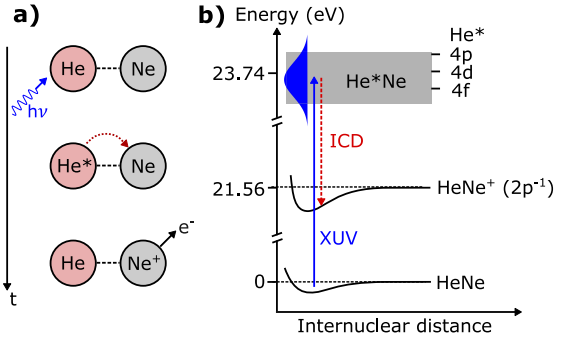

Figure 1. Resonant ICD in the HeNe dimer. (a) Excitation of the He site with a high-energy photon is followed by an energy transfer to the Ne site, leading to the ejection of a 2*p* electron. (b) Sketch of the relevant energy levels of HeNe along with the XUV excitation scheme (blue arrow) and the ICD (red dashed arrow). The congested potential energy curves correlating to the *p*-, *d*-, and *f*-asymptotes are indicated by the gray-shaded area.

der Waals complex (ground-state binding energy 2 meV, equilibrium distance 3 Å[30]). The He site is optically excited to the states correlated to the He $n = 4$ asymptote (23.7 eV) lying below the ionization potential (IP) of He (24.59 eV) but above the IP of Ne (21.56 eV). Subsequent energy transfer between the two sites leads to the ejection of a 2*p* electron from the Ne site.

The process is probed using XUV-WPI. The technique is schematically described in Figure 2. Each of the two phase-coherent XUV pulses excites a specific pathway in the sample

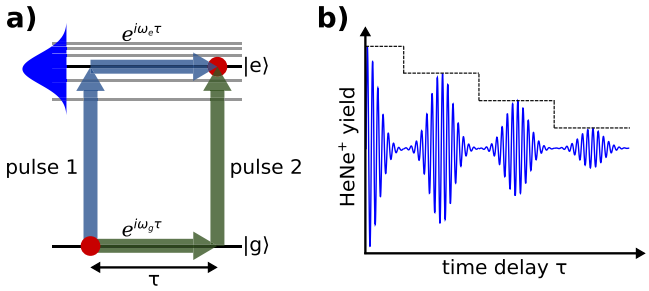

Figure 2. WPI scheme. (a) Excitation pathways of pulses 1 and 2 accumulate different phase factors ($\exp[i\omega_j\tau]$, $j = g, e$) as a function of the pulse delay τ which leads to a characteristic interference pattern in the ion yield, as schematically shown in (b). The dashed line indicates the expected stepwise decoherence caused by the ICD of the system.

leading to the same final state. Since the two pathways evolve along different states during the pulse delay τ, they accumulate different phase factors, giving rise to destructive/constructive interference in the final state. The ICD rate reflects the population of the $n = 4$ state manifold and, thus, maps the pathway interference onto the $HeNe^+$ yield (Figure 2b), which is detected in the experiment. The superposition of many pathways excited within the laser bandwidth leads to a complex beat spectrum, which exhibits dephasing and rephasing recurrences and an overall decay due to the decoherence of the system (Figure 2b). In addition, the Fourier transform of the interference fringes provides the excitation spectrum of the sample[1] with a frequency resolution that can exceed the laser bandwidth by orders of magnitude.[31] We note that this information can be also gained with a frequency-domain absorption experiment.[29] Yet, the time-domain WPI approach allows adding a separated probe process to clock the system's dynamics correlated to the spectrally resolved excitations, thus offering high spectro-temporal resolution. The deferred probe process is usually performed with a third laser pulse photoionizing the system. In the current study, the ICD process instead serves as the probe step, leading to the ionization of the system.

Vibronic interferometry requires the control of the relative phase/delay of the excitation pulses to a fraction of the fringe period (hc/λ_{XUV}), which is particularly challenging to achieve at XUV wavelengths, for which the fringe period is on the order of 100−200 as. This is in contrast to the study of pure vibrational WP beatings, where the fringe periods are typically two to three orders of magnitude longer, and thus demands on phase stability are greatly relaxed. We solve the problem with a specialized XUV phase-cycling scheme.[10] In this scheme, shot-to-shot cycling of the relative carrier-envelope phase between the XUV pulses is implemented, which leads to a low-frequency beat note (here ∼1 Hz) in the ion yield. Heterodyne lock-in detection is applied using an optical interference signal as the reference waveform for lock-in amplification. This detection scheme leads to the downshift of the fringe frequencies by 2−4 orders of magnitude (to 10−100 fs), which greatly simplifies the sampling of the interference fringes in the time domain. At the same time, the heterodyne detection eliminates most of the phase noise in the signal. Thus, it provides a passive interferometer stabilization sufficient for interferometry in the XUV domain. As well, background contributions are efficiently suppressed by the lock-in detection technique, which greatly improves the sensitivity. More details can be found in refs 4, 10, and 31.

https://doi.org/10.1021/acs.jpclett.2c01619
J. Phys. Chem. Lett. 2022, 13, 8470−8476

The experiments were performed with the seeded free-electron laser (FEL) FERMI FEL-1[32] at the low-density-matter endstation.[33] A compact, highly stable phase-cycling interferometer[34] was implemented in the seed-laser beam path for double-pulse seeding[35] of the high-gain harmonic generation (HGHG) process (Figure 3a). This approach enabled the generation of two XUV pulses with the phase properties controlled by those of the seed. Special attention was given to the preparation of the electron beam phase space driving the FEL amplification process. The energy-phase modulations in the beam were minimized, obtaining a region of a few hundred femtoseconds to accommodate the double pulses modulating the electron density and driving the amplification. In this way, two phase-coherent XUV pulses were generated at the fifth harmonic ($h\nu$ = 23.7 eV, $E_{pulse} \approx 12\ \mu$J, pulse duration: ≈45 fs, repetition rate: 50 Hz) whose relative phase was cycled at a rate of 9.3 Hz. No modification of the XUV beam path was necessary, and the pulses were automatically collinearly aligned, maximizing the interference contrast. The HeNe molecules were produced by coexpansion of a 94%/6% mixture of He and Ne gas through a home-built pulsed nozzle (nozzle temperature: 50 K, orifice diameter: 150 μm, opening time: 42 μs, stagnation pressure: 30 bar) (Figure 3a). The FEL pulses intersected with the molecular beam at right angles and the produced ions were recorded with an ion time-of-flight (iTOF) spectrometer. An exemplary mass spectrum obtained for resonant excitation of the HeNe molecule with a single XUV pulse ($h\nu$ = 23.66 eV) is shown in Figure 3b. Under these conditions, the $^{20}NeHe^+$ ion yield amounts to ≈9% of the $^{20}Ne^+$ contribution. Hence, less than 0.5% of the species in the gas expansion were HeNe dimers. For comparison, the pure $^{20}Ne_2^+$ ion yield was 19% of the $^{20}Ne^+$ yield (not shown).

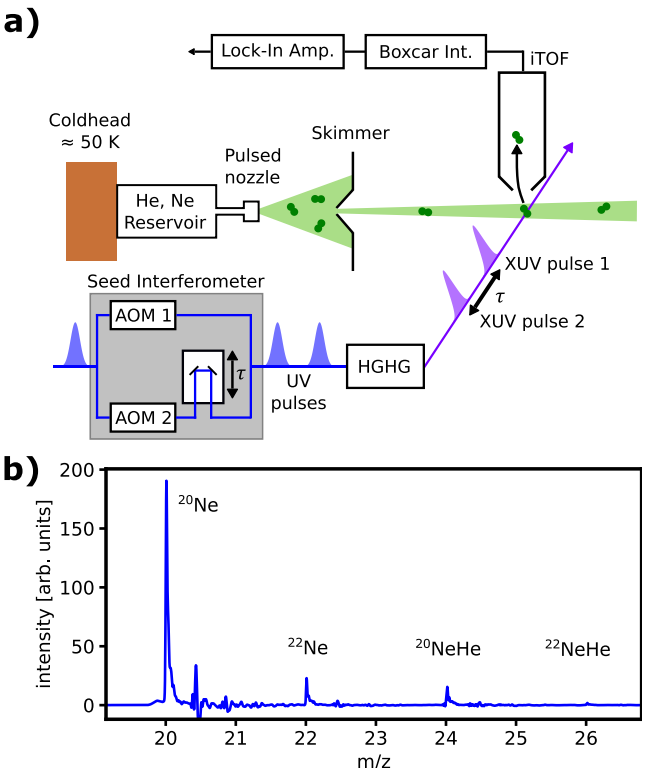

Figure 3. (a) Experimental setup. Phase-cycled seed laser pulses are generated in a Mach–Zehnder interferometer comprising an acousto-optical modulator (AOM1, AOM2) in each interferometer arm to control the relative phase between the pulses and a delay stage to control the interpulse delay τ. The UV seed pulses drive the high-gain harmonic generation (HGHG) in the FEL leading to phase-cycled XUV pulses. The iTOF signal is gated with a boxcar integrator and amplified with a lock-in amplifier. (b) Typical ion mass-to-charge (m/z) spectrum for a FEL photon energy of 23.66 eV. Amplification of the detector signal leads to overshoots in the mass spectrum visible, e.g., at m/z = 20.5.

The low HeNe particle density and the low signal rates posed particular challenges to the experiment. At the used photon energies, we find that only ≤3% of the ionized dimers carry an interferometric signal. In order to extract the interference signals from the mass spectra, the iTOF transients were filtered with a boxcar integrator selecting the $He^{20}Ne^+$ mass peak. This signal was fed into a lock-in amplifier to selectively amplify only the ion yield exhibiting the characteristic beat note imprinted by the phase cycling of the FEL pulses, while suppressing the background contributions from noninterferometric ionization processes. This enabled us to recover the XUV interference signal from the $HeNe^+$ ion yield despite the demanding experimental conditions of the required high phase stability and the dominant background ion yields (see also discussion to follow).

Figure 4a,b shows the interferometric transients for two different excitation energies. The interference fringes are clearly visible for interpulse delays of up to τ = 800 fs. We note that, for $\tau \leq$ 150 fs, optical interference of the seed pulses

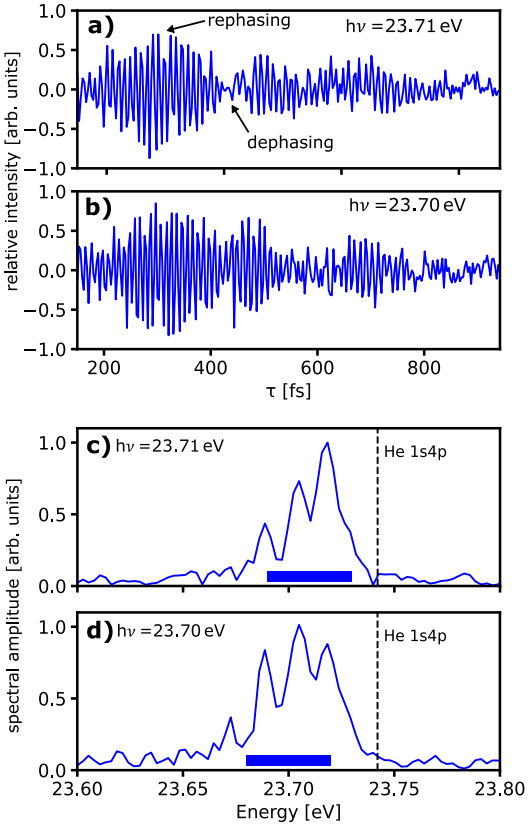

Figure 4. (a, b) Interference signals for photon energies $h\nu$ = 23.71 eV (a) and 23.70 eV (b). (c, d) Fourier spectra of the interference fringes. The FEL center wavelengths and spectral bandwidths (fwhm) are indicated by the blue bars, and the He $1s \rightarrow 4p$ resonances are indicated by the dashed lines.

https://doi.org/10.1021/acs.jpclett.2c01619
J. Phys. Chem. Lett. 2022, 13, 8470–8476

compromises the HGHG process and thus the measured interference signal.[36] Therefore, this region is not considered for the data analysis. The fringe frequency corresponds to the absorption frequency of individual vibronic transitions. Due to the heterodyne lock-in detection, the fringe period $\overline{T} \approx 10$ fs is much larger compared to the fully sampled case, where the fringe period would be $T \approx h/23.7$ eV = 175 as. Since many different, closely spaced states are excited simultaneously by the broadband XUV pulses, a complex fringe pattern emerges, exhibiting periodic rephasing maxima, which may be interpreted as vibronic WP revivals. A clear decay of the fringe amplitude can be identified within the observation window and is attributed to the decoherence caused by the ICD process (see below). We note that, for the excitation into $n = 3$, the ICD process leads to a dissociation of the dimer with a probability of ≈30%.[29,37] In the current study, we could not observe any interference signal or thus a signature for the ICD process in the Ne^+ yield, probably because of an insufficient signal-to-noise ratio.

For $n = 3$ excitation in HeNe, ICD decay times of ≤1 ps were deduced[29] from vibrational line broadenings and are much shorter than the natural lifetime of the excited states (∼nanoseconds). This suggests that also for the excitation to higher-lying asymptotic states of He (with $n > 3$), ICD is the dominating decay mechanism causing the decoherence of the interferometric transients in Figure 4a,b. Rotational dephasing might be another mechanism explaining the amplitude decay over time. In this case, a rephasing of the signal should occur at larger delays beyond the observation window of the current experiment. However, the short decay times deduced in the previous study provide a strong indication that the observed decay reflects the decoherence caused by the ICD of the system.

For the ICD rates, a strong dependence on the distance between the interacting constituents ($\propto 1/r^6$) is expected, leading to a nonexponential decay behavior.[38,39] Distinguishing different decay mechanisms based on the absorption line profiles is often difficult, and direct time-domain approaches are favorable in this case. Yet, so far, only few time-resolved experiments have been dedicated to the nonexponential decay behavior of ICD, where the dynamics were indirectly deduced in frequency-domain coincidence experiments,[40,41] however, not directly with femtosecond spectroscopy in the time domain. In principle, the WPI data contains information about the nuclear motion which would allow for the real-time mapping of the ICD rate in the time domain. Here, the strong distance dependence of ICD should lead to a stepwise amplitude decay for each round trip of the excited WPs on the potential energy curves (cf. Figure 2b). Accordingly, Figure 4a,b shows a clear amplitude decay on an ultrafast time scale. However, for a clear mapping of the nuclear motion and the decay behavior, a disentanglement of the contributions from the different vibrational and electronic states is needed. This might be achieved with accurate theory models in combination with an increased signal-to-noise level in the experiment. Likewise, a more selective excitation into specific electronic states using narrower XUV pulses may assist this interpretation.

In principle, conventional femtosecond XUV-pump, NIR-probe photoelectron/-ion spectroscopy should be able to map the pure vibrational WP beatings through the Franck−Condon window to higher-lying cationic states. Here, the ICD process should be observable as a loss in the photoionization yield by the probe pulse. We have attempted these measurements; however, we could not discern any vibrational beatings from the background ion yield. The large ionization background is explained by the nonresonant ionization of the molecule occurring for the excitation with broadband femtosecond laser pulses at photon energies above the Ne IP (>21.56 eV), triggering simultaneously the resonant ICD as well as the nonresonant ionization of the molecule. This is in contrast to narrow-band synchrotron excitation, where an enhancement of the ionization cross section by a factor of 60 was observed for resonant excitation to states correlated to the He $n = 3$ asymptote.[29] In the WPI experiments using broadband femtosecond pulses, the selectivity is greatly enhanced since only interference signals for the resonant excitation contribute outside of the temporal pulse overlap ($\tau \gtrsim 150$ fs) as shown in Figure 4 a,b. Such selectivity is not present in the conventional XUV-pump, NIR-probe experiments.

As another advantage, by Fourier analysis of the interferometric signal, spectral information beyond the laser bandwidth can be gained. Figure 4c,d shows the Fourier transforms of Figure 4a,b, revealing the excitation spectrum of the molecule for both laser wavelengths. To recover the absolute energy scale, a linear energy shift of the Fourier spectrum was applied to compensate for the frequency downshift of the heterodyne detection. Remarkably, the spectral resolution in the femtosecond interference experiment is 5.5 meV, which is a factor of 7.3 better than the spectral bandwidth of the FEL pulses and only a factor of 3.2 lower than in the high-resolution synchrotron absorption experiment.[29] The high density of electronic and vibrational states in the energy window excited with the femtosecond laser pulses leads to a well-resolved but complex vibronic spectrum. In analogy to the synchrotron experiment of the states with $n = 3$, calculations of the potential energy curves would provide insight into the individual spectral contributions. To the best of our knowledge, the states correlating to the He $n = 4$ asymptote have not been calculated for the HeNe dimer, and we therefore refrain in the current work from a further assignment of the spectral features. We note that, in the applied twin-seeding scheme, an energy chirp on the electron bunch can lead to shifted spectra for the second pulse (up to ≈20 meV) at large pulse delays as applied here. Hence, the amplitudes of the individual features in the Fourier spectrum (Figure 4c,d) may be slightly misleading. Likewise, the amplitude decay in the time domain might be influenced by this effect. This ambiguity might be reduced by a more careful preparation of the electron bunch and is expected to further improve in echo-enabled harmonic generation.[42]

In conclusion, we have used XUV interferometry to probe vibronic WP beatings in autoionizing states of the HeNe molecule on ultrafast time scales. The experiment provides a benchmark in sensitivity to probe highly dilute molecular quantum systems with WPI in the XUV domain and reveals the decoherence induced by ultrafast decay processes such as ICD. In contrast to narrowband synchrotron radiation, the broadband femtosecond laser excitation launches vibronic WPs extending over several vibrational and electronic states and thus may initiate a concerted motion of the nuclei. Combined with the demonstrated Fourier transform analysis, this opens up the possibility to study ICD and related ultrafast processes in real time with high temporal and spectral resolution. At the current state of the experiment, a stepwise (rather than smooth exponential) decoherence of the system due to ICD could not

https://doi.org/10.1021/acs.jpclett.2c01619
J. Phys. Chem. Lett. 2022, 13, 8470−8476

be unequivocally identified. This would require the precise modeling of the molecule's potential energy curves along with a simulation of the WP propagation and potentially an improvement in the signal-to-noise level of the experiment.

By adding an NIR ionization pulse in combination with photoelectron detection, the experiment could readily be extended to two-dimensional spectroscopy. Such experiments would provide further insights into ultrafast molecular dynamics and would be particularly beneficial for revealing spectral correlations. The experimental scheme is not restricted to seeded FELs and can also be applied in tabletop high-order harmonic generation (HHG),[11] where spectral bandwidths are much larger and interferometric schemes will be even more beneficial. The current study extending XUV-WPI to molecular targets and ultrafast dynamics demonstrates thus a promising step in several directions of all-XUV interferometry.

■ ASSOCIATED CONTENT

Supporting Information

The Supporting Information is available free of charge at https://pubs.acs.org/doi/10.1021/acs.jpclett.2c01619.

Transparent Peer Review report available (PDF)

■ AUTHOR INFORMATION

Corresponding Author

Lukas Bruder − *Institute of Physics, University of Freiburg, 79104 Freiburg, Germany;* orcid.org/0000-0001-9992-9925; Email: lukas.bruder@physik.uni-freiburg.de

Authors

Daniel Uhl − *Institute of Physics, University of Freiburg, 79104 Freiburg, Germany*

Andreas Wituschek − *Institute of Physics, University of Freiburg, 79104 Freiburg, Germany*

Rupert Michiels − *Institute of Physics, University of Freiburg, 79104 Freiburg, Germany*

Florian Trinter − *Institut für Kernphysik, J. W. Goethe-Universität, 60438 Frankfurt am Main, Germany; Molecular Physics, Fritz-Haber-Institut der Max-Planck-Gesellschaft, 14195 Berlin, Germany;* orcid.org/0000-0002-0891-9180

Till Jahnke − *Institut für Kernphysik, J. W. Goethe-Universität, 60438 Frankfurt am Main, Germany; European XFEL, 22869 Schenefeld, Germany*

Enrico Allaria − *Elettra-Sincrotrone Trieste S.C.p.A., 34149 Trieste, Italy*

Carlo Callegari − *Elettra-Sincrotrone Trieste S.C.p.A., 34149 Trieste, Italy;* orcid.org/0000-0001-5491-7752

Miltcho Danailov − *Elettra-Sincrotrone Trieste S.C.p.A., 34149 Trieste, Italy*

Michele Di Fraia − *Elettra-Sincrotrone Trieste S.C.p.A., 34149 Trieste, Italy*

Oksana Plekan − *Elettra-Sincrotrone Trieste S.C.p.A., 34149 Trieste, Italy;* orcid.org/0000-0002-4692-7018

Ulrich Bangert − *Institute of Physics, University of Freiburg, 79104 Freiburg, Germany*

Katrin Dulitz − *Institute of Physics, University of Freiburg, 79104 Freiburg, Germany;* orcid.org/0000-0003-0489-6038

Friedemann Landmesser − *Institute of Physics, University of Freiburg, 79104 Freiburg, Germany;* orcid.org/0000-0001-6748-8862

Moritz Michelbach − *Institute of Physics, University of Freiburg, 79104 Freiburg, Germany*

Alberto Simoncig − *Elettra-Sincrotrone Trieste S.C.p.A., 34149 Trieste, Italy*

Michele Manfredda − *Elettra-Sincrotrone Trieste S.C.p.A., 34149 Trieste, Italy*

Simone Spampinati − *Elettra-Sincrotrone Trieste S.C.p.A., 34149 Trieste, Italy*

Giuseppe Penco − *Elettra-Sincrotrone Trieste S.C.p.A., 34149 Trieste, Italy*

Richard James Squibb − *Department of Physics, University of Gothenburg, 41296 Gothenburg, Sweden*

Raimund Feifel − *Department of Physics, University of Gothenburg, 41296 Gothenburg, Sweden;* orcid.org/0000-0001-5234-3935

Tim Laarmann − *Deutsches Elektronen-Synchrotron DESY, 22607 Hamburg, Germany; The Hamburg Centre for Ultrafast Imaging CUI, 22761 Hamburg, Germany*

Marcel Mudrich − *Department of Physics and Astronomy, Aarhus University, 8000 Aarhus, Denmark;* orcid.org/0000-0003-4959-5220

Kevin C. Prince − *Elettra-Sincrotrone Trieste S.C.p.A., 34149 Trieste, Italy;* orcid.org/0000-0002-5416-7354

Giulio Cerullo − *IFN-CNR and Dipartimento di Fisica, Politecnico di Milano, 20133 Milano, Italy;* orcid.org/0000-0002-9534-2702

Luca Giannessi − *Elettra-Sincrotrone Trieste S.C.p.A., 34149 Trieste, Italy; Istituto Nazionale di Fisica Nucleare, Laboratori Nazionali di Frascati, 00044 Frascati, Roma*

Frank Stienkemeier − *Institute of Physics, University of Freiburg, 79104 Freiburg, Germany;* orcid.org/0000-0001-6014-8013

Complete contact information is available at: https://pubs.acs.org/10.1021/acs.jpclett.2c01619

Funding

Funding by the Bundesministerium für Bildung and Forschung (BMBF) *STAR* (05K19VF3), by the European Research Council (ERC) with the Advanced Grant *COCONIS* (694965), and by the Deutsche Forschungsgemeinschaft (DFG) RTG 2079 and RTG 2717 and the Research Unit FOR 1789 is acknowledged. Also, funding by the Swedish Research Council, by the Knut and Alice Wallenberg Foundation, Sweden, and by the Danish Council for Independent Research (Grant No. 1026-00299B) is acknowledged.

Notes

The authors declare no competing financial interest.

■ ACKNOWLEDGMENTS

We gratefully acknowledge the support of the FERMI staff.

■ REFERENCES

(1) Scherer, N. F.; Carlson, R. J.; Matro, A.; Du, M.; Ruggiero, A. J.; Romero-Rochin, V.; Cina, J. A.; Fleming, G. R.; Rice, S. A. Fluorescence-Detected Wave Packet Interferometry: Time Resolved Molecular Spectroscopy with Sequences of Femtosecond Phase-Locked Pulses. *J. Chem. Phys.* **1991**, *95*, 1487−1511.

(2) Ohmori, K. Wave-Packet and Coherent Control Dynamics. *Annu. Rev. Phys. Chem.* **2009**, *60*, 487−511.

(3) Lomsadze, B.; Smith, B. C.; Cundiff, S. T. Tri-Comb Spectroscopy. *Nat. Photon* **2018**, *12*, 676.

(4) Tekavec, P. F.; Lott, G. A.; Marcus, A. H. Fluorescence-Detected Two-Dimensional Electronic Coherence Spectroscopy by Acousto-Optic Phase Modulation. *J. Chem. Phys.* **2007**, *127*, 214307−214307−21.
(5) Bruder, L.; Bangert, U.; Binz, M.; Uhl, D.; Stienkemeier, F. Coherent Multidimensional Spectroscopy in the Gas Phase. *J. Phys. B: At. Mol. Opt. Phys.* **2019**, *52*, 183501.
(6) Mukamel, S.; Healion, D.; Zhang, Y.; Biggs, J. D. Multidimensional Attosecond Resonant X-Ray Spectroscopy of Molecules: Lessons from the Optical Regime. *Annu. Rev. Phys. Chem.* **2013**, *64*, 101−127.
(7) Prince, K. C.; Allaria, E.; Callegari, C.; Cucini, R.; De Ninno, G.; Di Mitri, S.; Diviacco, B.; Ferrari, E.; Finetti, P.; Gauthier, D.; et al. Coherent Control with a Short-Wavelength Free-Electron Laser. *Nat. Photon* **2016**, *10*, 176−179.
(8) Jansen, G. S. M.; Rudolf, D.; Freisem, L.; Eikema, K. S. E.; Witte, S. Spatially Resolved Fourier Transform Spectroscopy in the Extreme Ultraviolet. *Optica* **2016**, *3*, 1122.
(9) Usenko, S.; Przystawik, A.; Jakob, M. A.; Lazzarino, L. L.; Brenner, G.; Toleikis, S.; Haunhorst, C.; Kip, D.; Laarmann, T. Attosecond Interferometry with Self-Amplified Spontaneous Emission of a Free-Electron Laser. *Nat. Commun.* **2017**, *8*, 15626.
(10) Wituschek, A.; Bruder, L.; Allaria, E.; Bangert, U.; Binz, M.; Borghes, R.; Callegari, C.; Cerullo, G.; Cinquegrana, P.; Giannessi, L.; et al. Tracking Attosecond Electronic Coherences Using Phase-Manipulated Extreme Ultraviolet Pulses. *Nat. Commun.* **2020**, *11*, 883.
(11) Wituschek, A.; Kornilov, O.; Witting, T.; Maikowski, L.; Stienkemeier, F.; Vrakking, M. J. J.; Bruder, L. Phase Cycling of Extreme Ultraviolet Pulse Sequences Generated in Rare Gases. *New J. Phys.* **2020**, *22*, 092001.
(12) Kaneyasu, T.; Hikosaka, Y.; Fujimoto, M.; Iwayama, H.; Katoh, M. Electron Wave Packet Interference in Atomic Inner-Shell Excitation. *Phys. Rev. Lett.* **2021**, *126*, 113202.
(13) Bellini, M.; Cavalieri, S.; Corsi, C.; Materazzi, M. Phase-Locked, Time-Delayed Harmonic Pulses for High Spectral Resolution in the Extreme Ultraviolet. *Opt. Lett., OL* **2001**, *26*, 1010−1012.
(14) Cavalieri, S.; Eramo, R.; Materazzi, M.; Corsi, C.; Bellini, M. Ramsey-Type Spectroscopy with High-Order Harmonics. *Phys. Rev. Lett.* **2002**, *89*, 133002.
(15) Koll, L.-M.; Maikowski, L.; Drescher, L.; Witting, T.; Vrakking, M. J. J. Experimental Control of Quantum-Mechanical Entanglement in an Attosecond Pump-Probe Experiment. *Phys. Rev. Lett.* **2022**, *128*, 043201.
(16) Bencivenga, F.; Cucini, R.; Capotondi, F.; Battistoni, A.; Mincigrucci, R.; Giangrisostomi, E.; Gessini, A.; Manfredda, M.; Nikolov, I. P.; Pedersoli, E.; et al. Four-Wave Mixing Experiments with Extreme Ultraviolet Transient Gratings. *Nature* **2015**, *520*, 205−208.
(17) Cao, W.; Warrick, E. R.; Fidler, A.; Neumark, D. M.; Leone, S. R. Noncollinear Wave Mixing of Attosecond XUV and Few-Cycle Optical Laser Pulses in Gas-Phase Atoms: Toward Multidimensional Spectroscopy Involving XUV Excitations. *Phys. Rev. A* **2016**, *94*, 053846.
(18) Foglia, L.; Capotondi, F.; Mincigrucci, R.; Naumenko, D.; Pedersoli, E.; Simoncig, A.; Kurdi, G.; Calvi, A.; Manfredda, M.; Raimondi, L. First Evidence of Purely Extreme-Ultraviolet Four-Wave Mixing. *Phys. Rev. Lett.* **2018**, *120*, 263901.
(19) Rouxel, J. R.; Fainozzi, D.; Mankowsky, R.; Rösner, B.; Seniutinas, G.; Mincigrucci, R.; Catalini, S.; Foglia, L.; Cucini, R.; Döring, F.; et al. Hard X-ray Transient Grating Spectroscopy on Bismuth Germanate. *Nat. Photonics* **2021**, *15*, 499−503.
(20) Uhl, D.; Wituschek, A.; Bangert, U.; Binz, M.; Callegari, C.; Di Fraia, M.; Plekan, O.; Prince, K. C.; Cerullo, G.; Giannessi, L.; et al. Improved Stabilization Scheme for Extreme Ultraviolet Quantum Interference Experiments. *J. Phys. B: At. Mol. Opt. Phys.* **2022**, *55*, 074002.
(21) Okino, T.; Furukawa, Y.; Nabekawa, Y.; Miyabe, S.; Eilanlou, A. A.; Takahashi, E. J.; Yamanouchi, K.; Midorikawa, K. Direct Observation of an Attosecond Electron Wave Packet in a Nitrogen Molecule. *Science* **2015**, *1*, e1500356.
(22) Carpeggiani, P. A.; Tzallas, P.; Palacios, A.; Gray, D.; Martín, F.; Charalambidis, D. Disclosing Intrinsic Molecular Dynamics on the 1-Fs Scale through Extreme-Ultraviolet Pump-Probe Measurements. *Phys. Rev. A* **2014**, *89*, 023420.
(23) Paul, P. M.; Toma, E. S.; Breger, P.; Mullot, G.; Augé, F.; Balcou, P.; Muller, H. G.; Agostini, P. Observation of a Train of Attosecond Pulses from High Harmonic Generation. *Science* **2001**, *292*, 1689−1692.
(24) Plunkett, A.; Alarcón, M. A.; Wood, J. K.; Greene, C. H.; Sandhu, A. Raman Interferometry between Autoionizing States to Probe Ultrafast Wave-Packet Dynamics with High Spectral Resolution. *Phys. Rev. Lett.* **2022**, *128*, 083001.
(25) Uhl, D.; Bangert, U.; Bruder, L.; Stienkemeier, F. Coherent Optical 2D Photoelectron Spectroscopy. *Optica* **2021**, *8*, 1316−1324.
(26) Fano, U. Effects of Configuration Interaction on Intensities and Phase Shifts. *Phys. Rev.* **1961**, *124*, 1866−1878.
(27) Cederbaum, L. S.; Zobeley, J.; Tarantelli, F. Giant Intermolecular Decay and Fragmentation of Clusters. *Phys. Rev. Lett.* **1997**, *79*, 4778−4781.
(28) Jahnke, T.; Hergenhahn, U.; Winter, B.; Dörner, R.; Frühling, U.; Demekhin, P. V.; Gokhberg, K.; Cederbaum, L. S.; Ehresmann, A.; Knie, A.; et al. Interatomic and Intermolecular Coulombic Decay. *Chem. Rev.* **2020**, *120*, 11295−11369.
(29) Trinter, F.; Williams, J. B.; Weller, M.; Waitz, M.; Pitzer, M.; Voigtsberger, J.; Schober, C.; Kastirke, G.; Müller, C.; Goihl, C.; et al. Vibrationally Resolved Decay Width of Interatomic Coulombic Decay in HeNe. *Phys. Rev. Lett.* **2013**, *111*, 233004.
(30) Cybulski, S. M.; Toczyłowski, R. R. Ground State Potential Energy Curves for He2, Ne2, Ar2, He−Ne, He−Ar, and Ne−Ar: A Coupled-Cluster Study. *J. Chem. Phys.* **1999**, *111*, 10520−10528.
(31) Bruder, L.; Mudrich, M.; Stienkemeier, F. Phase-Modulated Electronic Wave Packet Interferometry Reveals High Resolution Spectra of Free Rb Atoms and Rb*He Molecules. *Phys. Chem. Chem. Phys.* **2015**, *17*, 23877−23885.
(32) Allaria, E.; Badano, L.; Bassanese, S.; Capotondi, F.; Castronovo, D.; Cinquegrana, P.; Danailov, M. B.; D'Auria, G.; Demidovich, A.; De Monte, R.; et al. The FERMI Free-Electron Lasers. *J. Synchrotron Rad* **2015**, *22*, 485−491.
(33) Lyamayev, V.; Ovcharenko, Y.; Katzy, R.; Devetta, M.; Bruder, L.; LaForge, A.; Mudrich, M.; Person, U.; Stienkemeier, F.; Krikunova, M.; et al. A Modular End-Station for Atomic, Molecular, and Cluster Science at the Low Density Matter Beamline of FERMI@Elettra. *J. Phys. B: At. Mol. Opt. Phys.* **2013**, *46*, 164007.
(34) Wituschek, A.; Bruder, L.; Klein, L.-S.; Strucka, J.; Demidovich, A.; Danailov, M. B.; Stienkemeier, F. Stable Interferometric Platform for Phase Modulation of Seeded Free-Electron Lasers. *Opt. Lett.* **2019**, *44*, 943.
(35) Gauthier, D.; Ribič, P. R.; de Ninno, G.; Allaria, E.; Cinquegrana, P.; Danailov, M. B.; Demidovich, A.; Ferrari, E.; Giannessi, L. Generation of Phase-Locked Pulses from a Seeded Free-Electron Laser. *Phys. Rev. Lett.* **2016**, *116*, 024801.
(36) Wituschek, A.; Bruder, L.; Allaria, E.; Bangert, U.; Binz, M.; Callegari, C.; Cinquegrana, P.; Danailov, M.; Demidovich, A.; Fraia, M. D.; et al. High-Gain Harmonic Generation with Temporally Overlapping Seed Pulses and Application to Ultrafast Spectroscopy. *Opt. Express, OE* **2020**, *28*, 29976−29990.
(37) Mhamdi, A.; Trinter, F.; Rauch, C.; Weller, M.; Rist, J.; Waitz, M.; Siebert, J.; Metz, D.; Janke, C.; Kastirke, G.; et al. Resonant Interatomic Coulombic Decay in HeNe: Electron Angular Emission Distributions. *Phys. Rev. A* **2018**, *97*, 053407.
(38) Santra, R.; Zobeley, J.; Cederbaum, L. S.; Moiseyev, N. Interatomic Coulombic Decay in van Der Waals Clusters and Impact of Nuclear Motion. *Phys. Rev. Lett.* **2000**, *85*, 4490−4493.
(39) Rist, J.; Miteva, T.; Gaire, B.; Sann, H.; Trinter, F.; Keiling, M.; Gehrken, N.; Moradmand, A.; Berry, B.; Zohrabi, M.; et al. A Comprehensive Study of Interatomic Coulombic Decay in Argon

https://doi.org/10.1021/acs.jpclett.2c01619
J. Phys. Chem. Lett. 2022, 13, 8470−8476

Dimers: Extracting R-dependent Absolute Decay Rates from the Experiment. *Chem. Phys.* **2017**, *482*, 185−191.
(40) Frühling, U.; Trinter, F.; Karimi, F.; Williams, J. B.; Jahnke, T. Time-Resolved Studies of Interatomic Coulombic Decay. *J. Electron Spectrosc. Relat. Phenom.* **2015**, *204*, 237−244.
(41) Trinter, F.; Miteva, T.; Weller, M.; Hartung, A.; Richter, M.; Williams, J. B.; Gatton, A.; Gaire, B.; Sartor, J.; L. Landers, A.; et al. Ultrafast Temporal Evolution of Interatomic Coulombic Decay in NeKr Dimers. *Chem. Sci.* **2022**, *13*, 1789−1800.
(42) Rebernik Ribič, P.; Abrami, A.; Badano, L.; Bossi, M.; Braun, H.-H.; Bruchon, N.; Capotondi, F.; Castronovo, D.; Cautero, M.; Cinquegrana, P.; et al. Coherent Soft X-ray Pulses from an Echo-Enabled Harmonic Generation Free-Electron Laser. *Nat. Photon* **2019**, *13*, 555−561.

https://doi.org/10.1021/acs.jpclett.2c01619
J. Phys. Chem. Lett. 2022, 13, 8470−8476